10-31-2013

Interface states in CoFe2O4 spin-filter tunnel junctions

Pavel V. Lukashev
University of Nebraska-Lincoln, pavel.lukashev@uni.edu

John D. Burton
University of Nebraska-Lincoln, jburton2@unl.edu

Alexander Smogunov
CEA, Institut Rayonnement Matiere de Saclay, France

Julian P. Velev
University of Puerto Rico-San Juan, julian.velev@unl.edu

Evgeny Y. Tsymbal
University of Nebraska-Lincoln, tsymbal@unl.edu

Interface states in $CoFe_2O_4$ spin-filter tunnel junctions

Pavel V. Lukashev,[1,*] J. D. Burton,[1] Alexander Smogunov,[2] Julian P. Velev,[3] and Evgeny Y. Tsymbal[1,†]

[1]*Department of Physics and Astronomy & Nebraska Center for Materials and Nanoscience, University of Nebraska, Lincoln, Nebraska 68588, USA*

[2]*CEA, Institut Rayonnement Matière de Saclay, SPCSI, F-91191 Gif-sur-Yvette Cedex, France*

[3]*Department of Physics, Institute for Functional Nanomaterials, University of Puerto Rico, San Juan, Puerto Rico 00931, USA*

(Received 9 August 2013; published 31 October 2013)

Spin-filter tunneling is a promising way to generate highly spin-polarized current, a key component for spintronics applications. In this paper we explore the tunneling conductance across the spin-filter material $CoFe_2O_4$ interfaced with Au electrodes, a geometry which provides nearly perfect lattice matching at the $CoFe_2O_4$/Au(001) interface. Using density functional theory calculations we demonstrate that interface states play a decisive role in controlling the transport spin polarization in this tunnel junction. For a realistic $CoFe_2O_4$ barrier thickness, we predict a tunneling spin polarization of about −60%. We show that this value is lower than what is expected based solely on considerations of the spin-polarized band structure of $CoFe_2O_4$, and therefore that these interface states can play a detrimental role. We argue that this is a rather general feature of ferrimagnetic ferrites and could make an important impact on spin-filter tunneling applications.

DOI: 10.1103/PhysRevB.88.134430 PACS number(s): 72.25.−b, 73.40.Gk, 75.47.Lx

I. INTRODUCTION

In the past few decades spintronics has been one of the most active fields in condensed matter physics, mostly because of its vast potential for device applications.[1] The cornerstone of spintronics is the generation, injection, and transport of spin-polarized currents. The conventional approach is based on magnetic tunnel junctions (MTJs) in which two ferromagnetic electrodes are separated by a nonmagnetic insulating barrier. In MTJs the tunneling current depends on the relative magnetization orientation of the electrodes, an effect known as tunneling magnetoresistance (TMR).[2] An alternative approach is to use spin-filter tunneling where a ferromagnet (ferrimagnet) is used as a barrier in a tunnel junction with nonmagnetic electrodes.[3] Spin-filter tunneling relies on different probabilities for electrons with opposite spin to be transmitted through a spin-dependent energy barrier of the ferromagnetic (ferrimagnetic) insulator. The spin dependence of the energy barrier is due to the exchange splitting of the band structure, which leads to the conduction band minimum (CBM) and/or the valence band maximum (VBM) lying at different energies for majority- and minority-spin electrons. The tunneling transmission depends exponentially on the barrier height, and therefore the tunneling conductance is expected to be spin dependent.

Despite some promising early experiments on Eu chalcogenides, such as EuS,[4] EuSe,[5] and EuO,[6] demonstrating the potential of spin-filter tunneling using the Tedrow-Meservey technique,[7] practical applications are limited due to their low Curie temperatures. For that reason, recently the focus has shifted to spinel-based materials, such as $CoFe_2O_4$,[8,9] $NiFe_2O_4$,[10] $NiMn_2O_4$,[11] $BiMnO_3$,[12] $CoCr_2O_4$,[13] and $MnCr_2O_4$,[8] which exhibit much higher Curie temperatures.

The theoretical understanding of spin-filter tunneling has been largely based on the free-electron model[3,14] and more recently on the analysis of the complex band structure[15–18] of the spin-filter material.[19–21] In the former, the spin-filter efficiency is entirely determined by the spin-dependent barrier height in the ferromagnetic insulator. The latter approach takes into account the realistic electronic structure of the bulk material, in particular, the orbital character and symmetry of the complex bands. Both approaches work, at best, in the limit of large barrier thickness, thereby neglecting any possible effects of the electrode/barrier interfaces. In particular, the presence of localized interface states is known to play a decisive role in spin-dependent tunneling.[22,23] This question has yet to be addressed for spin-filter systems.

In this paper we employ density functional theory (DFT) calculations to explore spin filtering in a prototype Au/$CoFe_2O_4$/Au (001) tunnel junction. $CoFe_2O_4$ (CFO) has a much narrower minority-spin band gap,[9] and hence strong spin filtering with a large negative spin polarization is expected for a large thickness of CFO. We demonstrate, however, that majority-spin states present at the $CoFe_2O_4$/Au interface can produce a sizable contribution to the tunneling conductance for reasonable barrier thicknesses (i.e., ∼2 nm), thereby reducing the spin polarization anticipated from the complex band structure of bulk CFO alone. We demonstrate that these interface states originate from native surface states of CFO. We argue that such interface states are a rather general feature of ferrimagnetic ferrites and will have an important impact on spin-filter tunneling.

II. COMPUTATIONAL DETAILS

We perform DFT calculations using the QUANTUM ESPRESSO (QE) package.[24] We use the generalized gradient approximation (GGA) according to the Perdew-Burke-Ernzerhof (PBE) formulation[25] with an energy cutoff of 500 eV for the plane-wave expansion and a k-point sampling of $6 \times 6 \times 4$ (bulk $CoFe_2O_4$) and $4 \times 4 \times 1$ (heterostructure) for the self-consistent calculations. Tunneling transmission through a $CoFe_2O_4$ (CFO) barrier separating two semi-infinite leads of Au is calculated using the wave-function-matching formalism implemented for plane waves and pseudopotentials in the QE package.[26,27] All calculations are performed with the Hubbard U correction,[28] which is necessary to accurately describe the insulating electronic structure of CFO.[29] We set $U = 3$ eV and

$J = 0$ eV for the d orbitals of both Fe and Co, in accordance with a recent theoretical study.[21] Analysis of the complex band structure is achieved by constructing Wannier orbitals from the GGA + U band structure of bulk CFO (Ref. 30) and using standard tight-binding techniques thereafter.

III. RESULTS

A. Bulk CFO

CFO is a ferrimagnetic insulator with a bulk Curie temperature of 796 K.[9] The oxygen atoms form a face-centered-cubic (fcc) sublattice, with cation atoms distributed over tetrahedrally and octahedrally coordinated sites. CFO has an inverse spinel structure with $Fd\bar{3}m$ symmetry with 56 atoms per cell. Fe atoms occupy all of the tetrahedral whereas the octahedral sites are randomly occupied by Co and Fe.[29] For a manageable computational cell we arrange the Co and Fe atoms on the octahedral sites in order to increase the symmetry of the cell. This allows a reduction in the size of the unit cell to a tetragonal cell of 28 atoms with space group *Imma*. In this geometry the calculated lattice parameters for the CFO are $a =$ 5.91 Å and $c/a = 1.41$.

The ground state of CFO is ferrimagnetic, where magnetic moments on octahedral sites are aligned parallel to one another, but antiparallel to the magnetic moments of Fe atoms at tetrahedral sites. The magnetic moments projected on individual atomic sites are $2.5\mu_B$ for Co, $4.0\mu_B$ for Fe at octahedral sites, and $-3.9\mu_B$ for Fe at tetrahedral sites. There are also induced magnetic moments on O atoms: $0.05\mu_B$ per O in the CoO_2 planes and $0.15\mu_B$ per O in the FeO_2 planes. The total magnetic moment of CFO is $3.0\mu_B$ per formula unit, consistent with the expected formal electronic configurations of the transition-metal cations (Co^{2+} and Fe^{3+} both in their high-spin configurations) and the ferrimagnetic alignment.

Figure 1(b) shows the calculated local densities of states (LDOS) for the bulk CFO, and Fig. 2 (middle panel) shows the band structure of the bulk CFO in the $\Gamma \rightarrow Z$ direction. We find that a band gap is about 0.8 eV, determined by minority-spin states, consistent with previous DFT + U calculations of CFO which reported band gaps in the range of 0.5–1 eV.[21,29,31] The exchange splitting of the CBM is $\Delta_{ex} = 0.9$ eV, consistent with previously reported values in the range of 0.5–1.2 eV.[21,29,31] The VBM is predominantly composed of Co (hybridized with O) states, while the CBM in both spin channels is composed of Fe states. Thus, Δ_{ex} is almost entirely due to the splitting between the Fe states on the octahedral and tetrahedral sites, in agreement with recently published data.[21]

B. CFO surface and interface states

Figure 1(a) shows an Au/CFO/Au supercell used in our calculations. We construct the supercell by lattice matching (001) oriented fcc Au with bulk CFO, leading to a tensile strain on the Au of less than 1%. We assume a CoO_2 termination of the CFO (001) layer and place interfacial Au atop O atoms. The supercell contains 8 formula units of CFO plus an additional monolayer (ML) of Co_2O_4 to ensure symmetric interface termination, resulting in nonstoichiometry of the CFO barrier. The structure is then fully optimized with a constrained in-plane lattice parameter of bulk CFO, $a = 5.91$ Å.

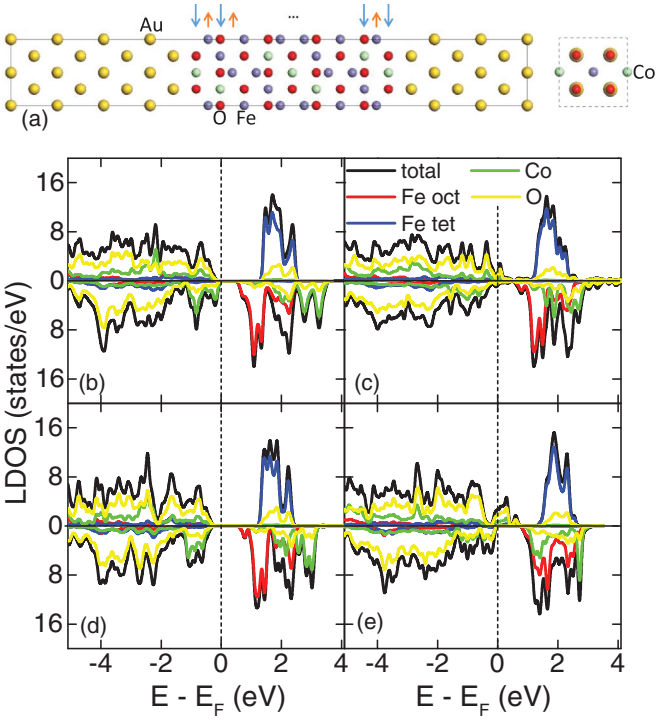

FIG. 1. (Color online) (a) Structural model for the Au/CFO/Au tunnel junction. The magnetic moment direction in each layer is indicated by the arrows. LDOS of (b) bulk CFO, (c) interfacial and (d) middle CFO layers of the Au/CFO/Au tunnel junction, and (e) the surface layer of a standalone (001) CFO slab. The green line represents octahedral Co, the red line octahedral Fe, the blue line tetrahedral Fe, the yellow line O, and the black line total LDOS. The majority- and minority-spin LDOS are displayed in the upper and lower panels, respectively. The vertical dashed lines denote the Fermi energy.

The calculated LDOS for the Au/CFO/Au tunnel junction is shown in Fig. 1 for interfacial [Fig. 1(c)] and middle [Fig. 1(d)] CFO layers. While the LDOS for the middle CFO layer closely resembles that of bulk [compare Figs. 1(b) and 1(d)], the interface LDOS exhibits different behavior.[32] As is evident from Fig. 1(c), interface states appear within the band gap of CFO for the majority-spin electrons, with a peak near the Fermi energy (E_F).

The CFO/Au interface states originate from native CFO (001) surface states, as confirmed from a separate calculation of a standalone CFO (001) slab with the same structure as in the supercell. The surface LDOS of this slab [Fig. 1(e)] displays surface states in the bulk gap for majority but not for minority spins. Details of the surface states are shown in Fig. 3. In Figs. 3(a)–3(c) the $\mathbf{k}_{\parallel}$-resolved LDOS is plotted in the two-dimensional Brillouin zone (2D BZ) for the surface atomic layer in the CFO (001) slab, calculated for the majority spin at different energies (see the figure caption). Figure 3(d) shows the majority-spin density for the (001) CFO slab calculated by integrating the surface layer LDOS from E_F to $E_F + 0.4$ eV. The majority-spin surface states mostly consist of O-p_x, O-p_y, and Co-d_{xy} orbitals, as shown in Fig. 3(d) and confirmed

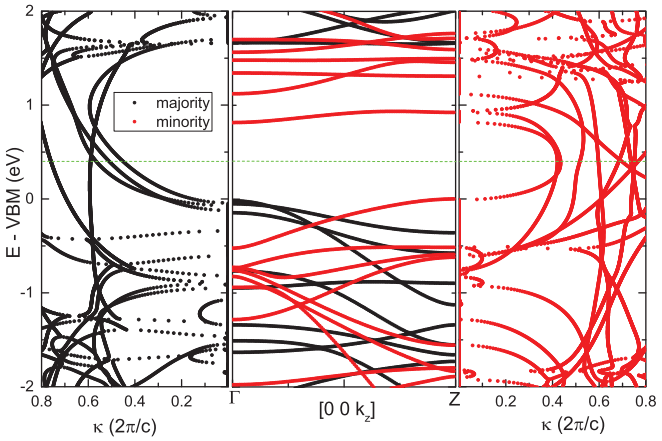

FIG. 2. (Color online) Spin-dependent complex band structure of CFO for $\mathbf{k}_\parallel = 0$ in the $\Gamma \rightarrow Z$ direction for majority spin (left panel) and minority spin (right panel). The middle panel shows real bands (black, majority; red, minority spin) for the same direction. The complex bands are connected to the real bands and inherit their symmetry properties. The curvature for complex and real bands is the same at the connecting points due to the analytic properties of the energy dispersion function $E(k_z)$. The dashed green line indicates the position of the Fermi level in the Au/CFO/Au tunnel junction.

by additional calculations of the orbital contributions to the $\mathbf{k}_\parallel$-resolved LDOS (not shown). These states originate from the fact that, at the surface, the Co atoms lose their octahedral coordination due to one "missing" O atom at the apex. The octahedral crystal field in the bulk splits the Co d states into a low energy t_{2g} and higher energy e_g manifold. Absence of the apex O atom at the surface further splits the e_g states

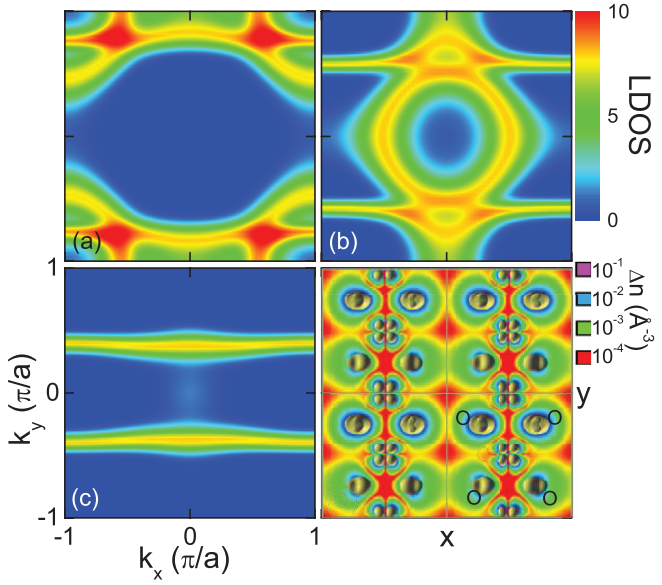

FIG. 3. (Color online) (a)–(c) $\mathbf{k}_\parallel$-resolved majority-spin LDOS (arbitrary units) at (a) E_F, (b) $E_F + 0.2$ eV, and (c) $E_F + 0.4$ eV for the surface atomic layer in the standalone (001) CFO slab. (d) Integrated LDOS, Δn, in real space for the surface layer of the (001) CFO slab from E_F to $E_F + 0.4$ eV. Color indicates the density on a plane cutting through the surface Co atoms and the shaded surfaces correspond to a constant density $\Delta n = 0.05$ Å^{-3}.

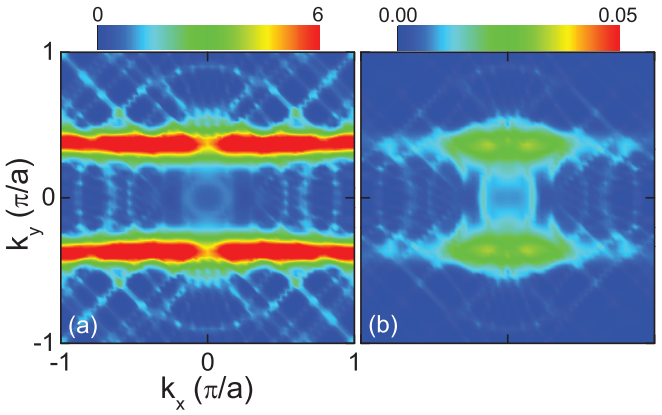

FIG. 4. (Color online) $\mathbf{k}_\parallel$-resolved majority-spin LDOS (arbitrary units) at the Fermi energy for (a) interfacial and (b) middle CFO layers in a Au/CFO/Au tunnel junction.

which make up the majority-spin VBM, lowering the d_{z^2} states and raising the d_{xy} states.[33] The higher crystal field of the d_{xy} orbitals leads to the formation of surface states. As seen in Fig. 3(d), the structure consists of relatively well-separated parallel chains of CoO_2 oriented along the y direction, leading to larger dispersion along y than x and therefore giving rise to the twofold rotational symmetry seen in Figs. 3(a)–3(c).

These majority-spin surface states survive at the Au/CFO interface, as can be seen in the $\mathbf{k}_\parallel$-resolved LDOS for the interfacial CFO layer, plotted in Fig. 4. As seen from Fig. 4(a), these states exhibit the same distinct stripelike features originating from the CFO surface states [compare Figs. 3(c) and 4(a)].[34] We note that the interface states shown of Fig. 4(a) are calculated at E_F of the Au/CFO/Au tunnel junction, which is shifted by about 0.25 eV away from the VBM in the (001) CFO slab. The surface states shown in Fig. 3(c) are plotted at $E_F + 0.4$ eV. The small energy difference is due to the slightly different nature of the LDOS at E_F for the CFO surface and interface. These majority-spin interface states of CFO in the Au/CFO/Au tunnel junction have a significant effect on the tunneling conductance across CFO, as confirmed below.

C. Conductance of Au/CFO/Au tunnel junctions

We calculate the tunneling conductance by taking the Au/CFO/Au supercell as a scattering region and attaching it on both sides to semi-infinite fcc Au leads. The calculations are performed at zero bias using a uniform 60×60 k-point mesh in the 2D BZ. The calculated conductance per unit cell area is $G_\uparrow = 0.11 \times 10^{-4} e^2/h$ for majority-spin channels and $G_\downarrow = 0.40 \times 10^{-4} e^2/h$ for minority-spin channels, respectively. The spin polarization of the tunneling current is $P = (G_\uparrow - G_\downarrow)/(G_\uparrow + G_\downarrow) = -57\%$. The negative sign of P is consistent with the expectation following from the lower minority-spin band gap compared to the majority-spin band gap.

Figures 5(a) and 5(b) show the $\mathbf{k}_\parallel$- and spin-resolved conductance of the Au/CFO/Au tunnel junction. The majority-spin conductance [Fig. 5(a)] can be explained by correlating it with the $\mathbf{k}_\parallel$-resolved LDOS shown in Fig. 4. The interface states

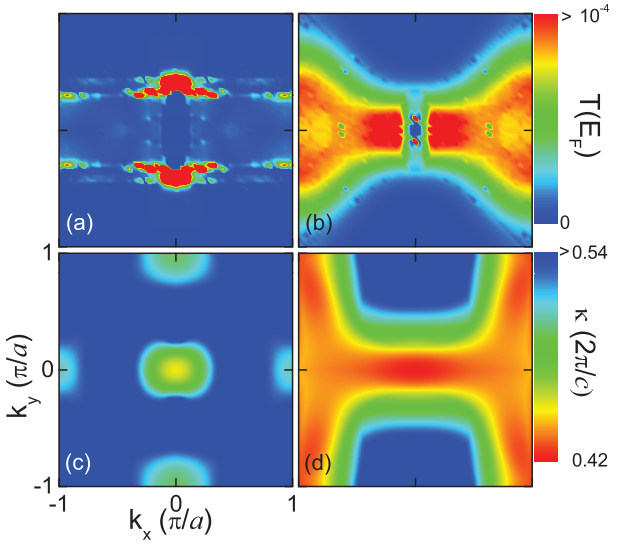

FIG. 5. (Color online) $\mathbf{k}_\parallel$-resolved transmission at E_F for (a) majority-spin channels and (b) minority-spin channels of the Au/CFO/Au tunnel junction. The lowest decay rate κ of the (c) majority-spin and (d) minority-spin evanescent states of bulk CFO as a function of $\mathbf{k}_\parallel$ in the 2D BZ at VBM + 0.4 eV.

seen in Fig. 4(a) as stripes for the interfacial CFO layer strongly decay away from the interface, however, even in the middle of the CFO barrier layer they do not completely vanish [Fig. 4(b)]. Moreover, a comparison of Fig. 5(a) with Fig. 4(b) indicates a clear correlation between the $\mathbf{k}_\parallel$-resolved conductance and LDOS profiles, both exhibiting maxima in the same area of the 2D BZ. The transmission distribution bears little resemblance, however, to the distribution of lowest decay rates for majority spins [Fig. 5(c)]. The latter are determined by the complex band structure shown in Fig. 2 for majority-spin (left panel) and minority-spin (right panel) electrons. We conclude, therefore, that the tunneling conductance of majority-spin electrons is, in fact, dominated by the interface states and therefore cannot be deduced by consideration of the complex band structure of CFO alone.

The conductance profile for the minority-spin electrons, on the other hand, is very reminiscent of the distribution of evanescent states in the band gap of CFO. Figure 5(d) shows the lowest decay rates of the minority-spin evanescent states in the band gap of CFO, where we see a close resemblance between the conductance [Fig. 5(b)] and the decay rate distribution [Fig. 5(d)] for the minority spin. Finally, we notice that both majority- and minority-spin channels demonstrate minimal conductance at the $\bar{\Gamma}$ point [Figs. 5(a) and 5(b)], which is somewhat inconsistent with the distribution of the decay rates [Figs. 5(c) and 5(d)] and with recently published results.[21] This is due to the mismatch of the band symmetries for both majority- and minority-spin channels of Au and CFO, calculated for $k_x = k_y = 0$, along the [001] direction. In particular, for Au along this direction there is only one band crossing the Fermi level, with orbital contributions s, p_z, and d_{z^2}. None of these orbital characters belong to the slowest decaying bands near the VBM of CFO, being primarily of p_y and d_{xy} orbital character for majority spin and $d_{x^2-y^2}$ and p_y for minority spin.

The contribution of the majority-spin interface states is detrimental to the net spin polarization of the tunneling conductance. To see this, we return to the simpler description of the spin-filter effect based solely on the complex band structure (Fig. 2) where we assume featureless electrodes and perfect interface transmission functions. In this case the conductance for each spin channel is determined by $G \propto \int e^{-2\kappa(\mathbf{k}_\parallel)t} d^2\mathbf{k}_\parallel$, where t is the thickness of the barrier, $\kappa\left(\mathbf{k}_\parallel\right)$ is the calculated lowest decay rate at E_F and $\mathbf{k}_\parallel$, as shown in Figs. 5(c) and 5(d), and the integral is over the entire 2D BZ. Using $t = 1.9$ nm and $E_F = \text{VBM} + 0.4$ eV, we find a spin polarization of $P = -80\%$. This is significantly larger than what is found from our full transport calculations, where interface states dominate the majority-spin channel.

The predicted effect of interface states on spin-polarized tunneling is not limited to the particular geometry of the tunnel junction considered above. We find that a terminating layer of the CFO (001) with a mixture of Fe and Co, as well as a purely FeO_2 terminating layer, both also lead to majority-spin interface states which produce similar detrimental effects on spin-polarized tunneling. One could expect a different behavior for Fe at tetrahedral sites comprising the interface; we find, however, that this termination is unstable.

Finally, we would like to mention the influence of defects in the tunneling barrier on spin-filter tunneling. Although this effect is not the subject of this paper, recent experiments have found a notable influence of oxygen vacancies[35] and other defects such as cationic disorder or antiphase boundaries[36] on the spin polarization of the tunneling current in the spin-filter experiments. Theoretical studies of this effect[37] would be very interesting to further elucidate critical factors affecting spin-filtering efficiency.

IV. SUMMARY AND CONCLUSIONS

In summary, we have shown that the spin polarization of the tunneling conductance in a Au/$CoFe_2O_4$/Au (001) tunnel junction is strongly affected by the majority-spin interface states, leading to a reduction in spin polarization as compared to expectations based on the spin-polarized band gap alone. Interface states are a general feature of the ferrimagnetic ferrites that are used as spin-filter barriers. Thus, the predicted effect has important implications for the design of spin-filter tunnel junctions, where the interface states need to be avoided to exploit the unspoiled spin filtering anticipated from the band structure of the bulk material.

ACKNOWLEDGMENTS

This research was supported by the NSF through Nebraska MRSEC (Grant No. DMR-0820521) and EPSCoR (Grant No. EPS-1010674) and the Nebraska Research Initiative. The work at the University of Puerto Rico was supported by NSF (Grants No. DMR-1105474 and No. EPS-1010094). Computations were performed at the University of Nebraska, Holland Computing Center.

*pavel.lukashev@unl.edu
†tsymbal@unl.edu

[1] *Handbook of Spin Transport and Magnetism*, edited by E. Y. Tsymbal and I. Žutić (CRC, Boca Raton, FL, 2011).
[2] E. Y. Tsymbal, O. N. Mryasov, and P. R. LeClair, J. Phys.: Condens. Matter **15**, R109 (2003).
[3] T. S. Santos and J. S. Moodera, in *Handbook of Spin Transport and Magnetism in Electronic Systems*, edited by E. Y. Tsymbal and I. Žutić (CRC, Boca Raton, FL, 2011), Chap. 13, p. 251.
[4] J. S. Moodera, X. Hao, G. A. Gibson, and R. Meservey, Phys. Rev. Lett. **61**, 637 (1988).
[5] J. S. Moodera, R. Meservey, and X. Hao, Phys. Rev. Lett. **70**, 853 (1993).
[6] T. S. Santos and J. S. Moodera, Phys. Rev. B **69**, 241203(R) (2004).
[7] R. Meservey and P. M. Tedrow, Phys. Rep. **238**, 173 (1994).
[8] M. G. Chapline and S. X. Wang, Phys. Rev. B **74**, 014418 (2006).
[9] A. V. Ramos, M. J. Guittet, J. B. Moussy, R. Mattana, C. Deranlot, F. Petroff, and C. Gatel, Appl. Phys. Lett. **91**, 122107 (2007).
[10] U. Lüders, M. Bibes, K. Bouzehouane, E. Jacquet, J.-P. Contour, S. Fusil, J.-F. Bobo, J. Fontcuberta, A. Barthélémy, and A. Fert, Appl. Phys. Lett. **88**, 082505 (2006).
[11] B. B. Nelson-Cheeseman, R. V. Chopdekar, L. M. B. Alldredge, J. S. Bettinger, E. Arenholz, and Y. Suzuki, Phys. Rev. B **76**, 220410(R) (2007).
[12] M. Gajek, M. Bibes, A. Barthélémy, K. Bouzehouane, S. Fusil, M. Varela, J. Fontcuberta, and A. Fert, Phys. Rev. B **72**, 020406(R) (2005).
[13] R. V. Chopdekar, B. B. Nelson-Cheeseman, M. Liberati, E. Arenholz, and Y. Suzuki, Phys. Rev. B **83**, 224426 (2011).
[14] G.-X. Miao, M. Müller, and J. S. Moodera, Europhys. Lett. **88**, 47006 (2009); Phys. Rev. Lett. **102**, 076601 (2009).
[15] M. van Schilfgaarde and W. R. L. Lambrecht, in *1997 MRS Fall Meeting–Symposium R–Tight Binding Approach to Computational Materials Science*. MRS Proceedings No. 491 (Materials Research Society, Pittsburgh, 1997), p. 137.
[16] Ph. Mavropoulos, N. Papanikolaou, and P. H. Dederichs, Phys. Rev. Lett. **85**, 1088 (2000).
[17] W. H. Butler, X.-G. Zhang, T. C. Schulthess, and J. M. MacLaren, Phys. Rev. B **63**, 054416 (2001).
[18] J. P. Velev, K. D. Belashchenko, D. A. Stewart, M. van Schilfgaarde, S. S. Jaswal, and E. Y. Tsymbal, Phys. Rev. Lett. **95**, 216601 (2005).
[19] J. Zhang, X.-G. Zhang, and X. F. Han, Appl. Phys. Lett. **100**, 222401 (2012).
[20] P. V. Lukashev, A. L. Wysocki, J. P. Velev, M. van Schilfgaarde, S. S. Jaswal, K. D. Belashchenko, and E. Y. Tsymbal, Phys. Rev. B **85**, 224414 (2012).
[21] N. M. Caffrey, D. Fritsch, T. Archer, S. Sanvito, and C. Ederer, Phys. Rev B **87**, 024419 (2013).
[22] E. Y. Tsymbal, K. D. Belashchenko, J. Velev, S. S. Jaswal, M. van Schilfgaarde, I. I. Oleynik, and D. A. Stewart, Prog. Mater. Sci. **52**, 401 (2007).
[23] J. P. Velev, P. A. Dowben, E. Y. Tsymbal, S. J. Jenkins, and A. N. Caruso, Surf. Sci. Rep. **63**, 400 (2008).
[24] P. Giannozzi *et al.*, J. Phys.: Condens. Matter **21**, 395502 (2009).
[25] J. P. Perdew, K. Burke, and M. Ernzerhof, Phys. Rev. Lett. **77**, 3865 (1996).
[26] H. J. Choi and J. Ihm, Phys. Rev. B **59**, 2267 (1999).
[27] A. Smogunov, A. Dal Corso, and E. Tosatti, Phys. Rev. B **70**, 045417 (2004).
[28] A. I. Liechtenstein, V. I. Anisimov, and J. Zaanen, Phys. Rev. B **52**, R5467 (1995).
[29] D. Fritsch and C. Ederer, Phys. Rev. B **82**, 104117 (2010).
[30] D. Korotin, A. V. Kozhevnikov, S. L. Skornyakov, I. Leonov, N. Binggeli, V. I. Anisimov, and G. Trimarchi, Eur. Phys. J. B **65**, 91 (2008).
[31] Z. Szotek, W. M. Temmerman, D. Ködderitzsch, A. Svane, L. Petit, and H. Winter, Phys. Rev. B **74**, 174431 (2006).
[32] By symmetry DOS are slightly different at the right and left CFO interfaces, but the difference is small and ignored throughout the text.
[33] Here x and y to refer to the in-plane lattice vectors. These are rotated by 45° with respect to the usual coordinate system used to describe octahedrally coordinated transition metals. Therefore, in our notation, d_{xy} belongs to the e_g manifold, with lobes along the directions of O nearest neighbors as seen in Fig. 2(d).
[34] We note kaleidoscope-type patterns in Figs. 4(a) and 4(b) occurring due to the quantum-well states in the Au layer comprising the supercell. These features disappear in the $\mathbf{k}_\parallel$-resolved transmission [Figs. 5(a) and 5(b)] which is calculated using semi-infinite Au leads.
[35] A. V. Ramos, T. S. Santos, G. X. Miao, M.-J. Guittet, J.-B. Moussy, and J. S. Moodera, Phys. Rev. B **78**, 180402 (2008).
[36] S. Matzen, J.-B. Moussy, G. X. Miao, and J. S. Moodera, Phys. Rev. B **87**, 184422 (2013).
[37] J. P. Velev, K. D. Belashchenko, S. S. Jaswal, and E. Y. Tsymbal, Appl. Phys. Lett. **90**, 072502 (2007).